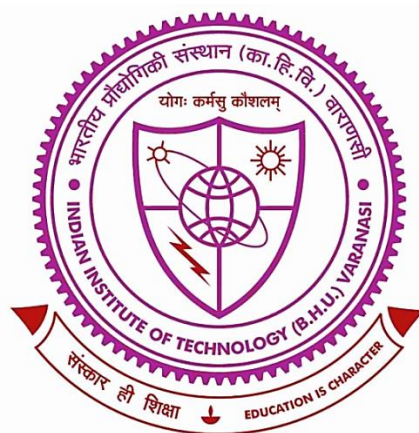


Targeting Antimicrobial Drug Resistance by Amine Functionalized Metal Nanoparticles



Thesis submitted for the
Award of Degree

DOCTOR OF PHILOSOPHY

BY

ATUL KUMAR TIWARI

Under the Supervision

Prof. P.C. Pandey

“Department of Chemistry”
Indian Institute of Technology
(Banaras Hindu University)

Varanasi-221005

India

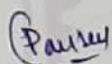
Roll No. 19051502

2023

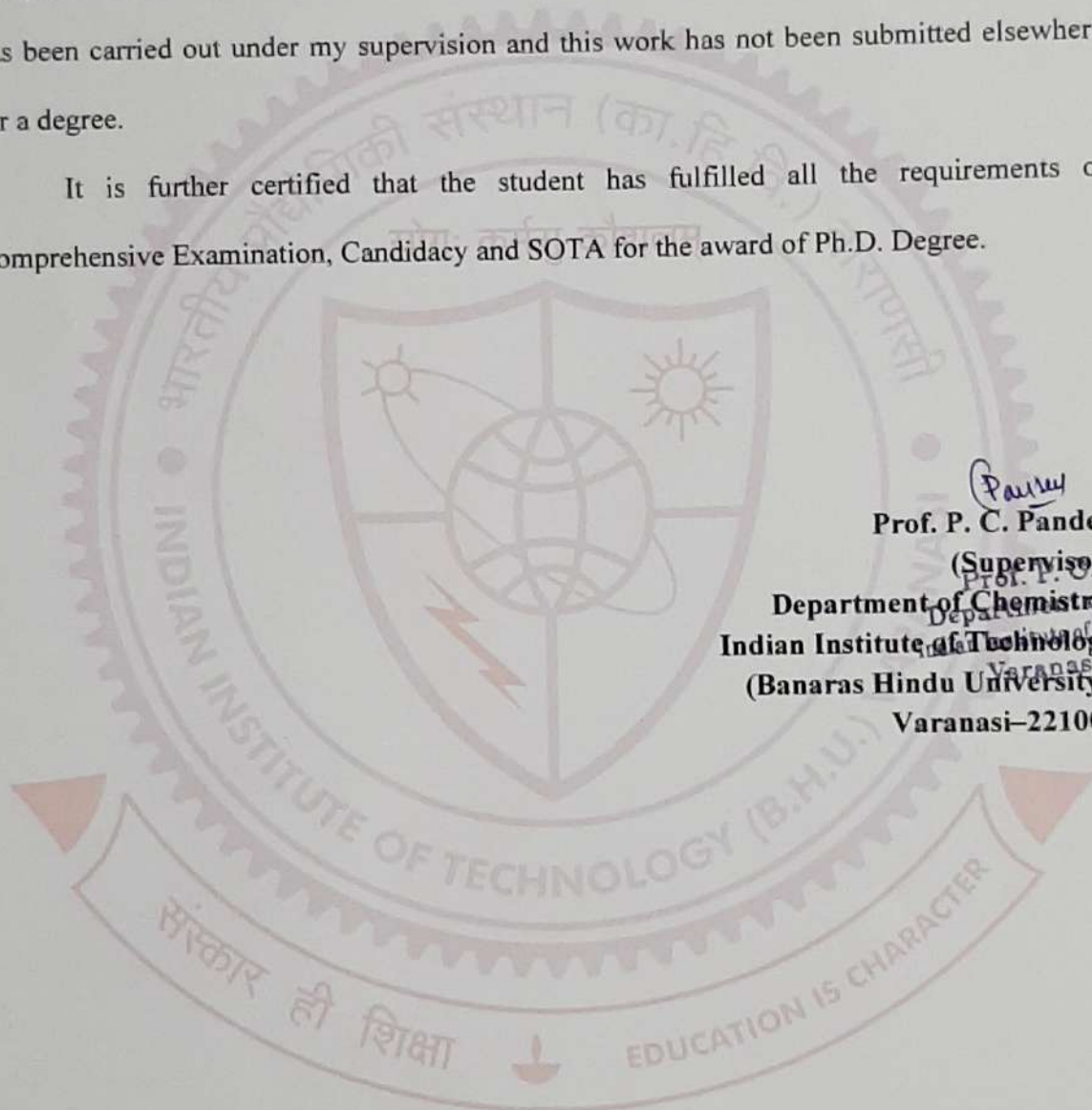
CERTIFICATE

It is certified that the work contained in the thesis titled "**Targeting Antimicrobial Drug Resistance by Amine Functionalized Metal Nanoparticles**" by **Atul Kumar Tiwari** has been carried out under my supervision and this work has not been submitted elsewhere for a degree.

It is further certified that the student has fulfilled all the requirements of Comprehensive Examination, Candidacy and SOTA for the award of Ph.D. Degree.


Prof. P. C. Pandey

(Supervisor)
Prof. P. C. Pandey
Department of Chemistry,
Indian Institute of Technology (BHU)
(Banaras Hindu University),
Varanasi-221005



DECLARATION BY THE CANDIDATE

I, "Atul Kumar Tiwari", certify that the work embodied in this thesis is my own bonafide work and carried out by me under the supervision of "Prof. P. C. Pandey" from "Even Sem. 2019-2020" to "Odd Sem. 2023-2024," at the Department of Chemistry, Indian Institute of Technology, (BHU), Varanasi. The matter embodied in this thesis has not been submitted for the award of any other degree/diploma. I declare that I have faithfully acknowledged and given credits to the research workers wherever their works have been cited in my work in this thesis. I further declare that I have not wilfully copied any other's work, paragraphs, text, data, results, etc., reported in journals, books, magazines, reports dissertations, theses, etc., or available at websites and have not included them in this thesis and have not cited as my own work.

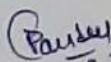
Date: 29/08/2023

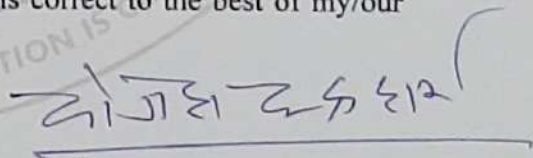
Place: Varanasi

Atul Kumar Tiwari
(Atul Kumar Tiwari)

CERTIFICATE BY THE SUPERVISOR

It is certified that the above statement made by the student is correct to the best of my/our knowledge.


Prof. P. C. Pandey
(Supervisor)
Department of Chemistry
Indian Institute of Technology
(Banaras Hindu University)
Varanasi- 221005


Prof. Y. C. Sharma
Head of Department
Department of Chemistry,
Indian Institute of Technology
(Banaras Hindu University),
Varanasi- 221005

विभागाध्यक्ष / HEAD
रसायन विज्ञान विभाग
Department of Chemistry
भारतीय प्रौद्योगिकी संस्थान (का.हि.वि.वि.)
Indian Institute of Technology (B.H.U.)
वाराणसी-२२१००५ / Varanasi-221005

COPYRIGHT TRANSFER CERTIFICATE

Title of the Thesis: Targeting Antimicrobial Drug Resistance by Amine Functionalized Metal Nanoparticles

Name of the Student: Atul Kumar Tiwari

Copyright Transfer

The undersigned hereby assigns to the Indian Institute of Technology (Banaras Hindu University) Varanasi all rights under copyright that may exist in and for the above thesis submitted for the award of the "Doctor of Philosophy" degree.

Date: 29/08/2023

Place: Varanasi

Atul Kumar Tiwari
(Atul Kumar Tiwari)

Note: However, the author may reproduce or authorize others to reproduce material extracted verbatim from the thesis or derivative of the thesis for author's personal use provided that the source and the Institute's copyright notice are indicated.

**DEDICATED TO MY LOVING
FAMILY...**

Acknowledgements

At the top and foremost, I am indebted to my greatest teacher of all that is almighty God. I realize that my present, past, and future are for a reason. Our culture has taught teachers' class is above the God therefore I am grateful to have Gurus in my life. I am deeply indebted to my spiritual Guru and founder of Banaras Hindu University, **Pt. Mahamana Madan Mohan Malviya Ji**, by his visionary thought the nation has eminent personalities.

To begin with, I “**Mr. Atul Kumar Tiwari**” would like to express my deep sense of gratitude to my supervisor “**Prof. P. C. Pandey**”, for providing me with generative, positive supervision, and for valuable guidance, constant support, critical and motivating comments throughout my research work.

I express my heartiest thanks to RPEC members, “**Prof. Y. C. Sharma**”, Department of Chemistry, IIT (BHU), Varanasi, “**Prof. Chandan Upadhyay**”, Department of School of Material Science and Technology, IIT (BHU), Varanasi for their valuable suggestions, constant guidance and kind encouragement during my research work.

My sincere thanks to the former Heads, “**Prof. Dhanesh Tiwary**” Department of Chemistry, IIT (BHU), Varanasi, the present head “**Prof Y.C. Sharma**” as well as all the faculty members of the Department of Chemistry IIT (BHU) for their kind support and for extending all required facilities to carry out my research work smoothly.

I gratefully acknowledge the facilities provided by **CIFC, IIT (BHU), CDC BHU, Varanasi**, and **SAIF, AIIMS, New Delhi**, for doing various characterization of samples.

My special thanks to my research collaborators “**Prof Roger J. Narayan**”, Joint Department of Biomedical Engineering, University of North Carolina, Chapel Hill, NC, United

States; and “**Dr. Munesh Kumar Gupta**” Department of Microbiology, IMS BHU, Varanasi who always encouraged me and promoted to next step.

I am extending my thanks to my colleagues “**Dr. Murli Dhar Mitra**”, **Mr. Hari Prakash Yadav**, and **Mrs. Manisha Pandey** for their valuable suggestions during my research work, and for creating an enjoyable lab ambiance and good memories, which I cherish forever.

I am thankful and indebted to **BRNS** and **IIT (BHU)** for providing me with financial support during my research work.

Finally, my parents, “**Smt. Kusum Lata Tiwari**” and “**Mr. Durga Prasad Tiwari**,” gave me my name, my life, and everything else in between. I pride myself on having my wife **Mrs. Anupa Mishra** and younger brother **Alok Tripathi** & Sister **Pooja Tiwari** for everything, but they truly shut me up when it comes down to describing how much I love them and appreciate the effort they have put into giving me the life I have now. They are the reason I did this, the reason I strive to be better. Their pride, for me, is my main goal in life.

Last but not least, I thank all my well-wishers and critics whose names I may have failed to mention here unintentionally. Thanks to all of you for being there for me when times were the toughest.

Date: 29/08/2023

Atul kumar tiwari

Place: Varanasi

(Atul Kumar Tiwari)



List of Symbols

3-APTMS	3-Aminopropyltrimethoxysilane
3-GPTMS	3-Glycidoxypropyltrimethoxysilane
PEI	Polyethyleneimine
HCl	Hydrogen Chloride
MDR	Multi-drug resistance
AgNPs	Silver nanoparticles
AuNPs	Gold nanoparticles
PdNPs	Palladium nanoparticles
MIC	Minimum Inhibitory concentration
MBC	Minimum bactericidal concentration
TEM	Transmission electron microscopy
HRSEM	High Resolution Scanning Electron Microscope
XPS	X-ray photoelectron spectroscopy
XRD	X-ray Diffraction
DLS	Dynamic light scattering
SAED	Selected area electron diffraction pattern
UV-Vis	Ultraviolet-Visible
FL Spectroscopy	Fluorescence Spectroscopy
λ	Wavelength
θ	Angle (degree)
Mw	Molecular weight
Mg	Milli gram



mM	Micro molar
nM	Nanomolar
Nm	Nanometer
mM	Millimolar
S	Time (second)
M	Minute
LOD	Limit of detection
OD	Optical density
PEI-AuNP@Van	Vancomycin Polyethyleneimine stabilized gold nanoparticle
FACS	Fluorescence-activated cell sorting
CLSM	Confocal laser scanning microscopy
BSA	Bovine Serum Albumin
Tyr	Tyrosine
Trp	Tryptophan



Contents

Title		Page No.
Title of Thesis		i
Certificate		ii
Declaration by the Candidate & Certificate by the Supervisor		iii
Copyright Transfer Certificate		iv
Dedication		v
Acknowledgment		vi-vii
List of Symbols		viii-ix
Contents		x-xx
List of Figures		xxi-xli
List of Schemes		xlii
List of Tables		xliii
Preface		xliv-xlvii
Chapter 1: General Introduction		1-43
1.1	Global scenario of Antimicrobial Drug resistance	1
1.2	The root cause of the evolution of antibiotic resistance among microbes	2
1.3	Synthesis and physicochemical properties of metal nanoparticles	5
1.4	Antimicrobial mechanism of metal nanoparticles: A detailed account	6



	1.4.1	Mechanism of cell membrane destruction and effect on membrane potential	8	
	1.4.2	Mechanism of nanoparticle-induced ROS generation and cellular damage	12	
	1.4.3	Inactivation of cellular proteins and enzymes	14	
	1.4.4	Molecular mechanism of DNA damage by metal nanoparticles.	17	
1.5	Metal nanoparticle-mediated eradication of bacterial biofilms		24	
	1.5.1	The biological dynamics of bacterial biofilms	24	
	1.5.2	Anti-biofilm mechanism of metal nanoparticles	27	
	1.5.3	Effect of physical properties of the metal nanoparticles on their anti-biofilm activity	28	
	1.5.4	The nanoparticle–biofilm interface	29	
		1.5.4.1	Mechanism of nanoparticle-mediated inhibition of bacterial quorum sensing cascades.	30
		1.5.4.2	Molecular interaction of metal nanoparticles with polymer matrix of biofilm.	32
1.6	Potential risk related to the application of metal nanoparticles as antimicrobial agents		35	
1.7	The potential implication of metal resistance		40	
	Motivation of Work and Objectives		44-45	
Chapter 2:				
Microwave-assisted rapid synthesis and effect of Organic Functionality on the antimicrobial activity of Noble metal nanoparticles			46-77	
	2.1	Introduction	46	
	2.2	Experimental section	48	



	2.2.1	Materials and reagent	48
	2.2.2	Bacterial strain	48
	2.2.3	Synthesis of alkoxy silane functionalized noble metal (mono-, bi- and tri-metallic) nanoparticles	49
	2.2.3.1	3-APTMS and cyclohexanone-mediated synthesis of AgNP-1 nanoparticles	49
	2.2.3.2	3-APTMS and 3-GPTMS-mediated synthesis of AgNP-2 nanoparticles	49
	2.2.3.3	3-APTMS and formaldehyde-mediated synthesis of AgNP-3 nanoparticles	49
	2.2.3.4	3-APTMS and cyclohexanone-mediated synthesis of AuNP-1 nanoparticles	50
	2.2.3.5	3-APTMS and 3-GPTMS-mediated synthesis of Au-NP-2 nanoparticles	50
	2.2.3.6	3-APTMS and cyclohexanone mediated sequential synthesis of Ag–Au–NP-1 bimetallic nanoparticles	50
	2.2.3.7	3-APTMS and 3-GPTMS-mediated simultaneous synthesis of Ag–Au–NP-2 bimetallic nanoparticles	50
	2.2.3.8	3-APTMS and cyclohexanone sequential synthesis of Pd–NP, and Pd–Ag bimetallic nanoparticles	51
	2.2.3.9	Sequential synthesis of Pd–Ag–Au trimetallic nanoparticles	51
	2.2.3.10	Characterization of functionalized Metal nanoparticles	52
	2.2.3.11	Assessment of antibacterial activity	52



		2.2.3.12	Assessment by agar well diffusion method	52
		2.2.3.13	Minimum inhibitory concentration and minimum bactericidal concentration	53
		2.2.3.14	Time kill assay	54
		2.2.3.15	Dose-dependent kill kinetic analysis	54
		2.2.3.16	Scanning electron microscopy	55
		2.2.3.17	Fluorescence spectroscopic studies	55
2.3	Results			56
	2.3.1	3-APTMS-mediated rapid synthesis of noble metal monometallic, bimetallic, and trimetallic nanoparticles		56
	2.3.2	Role of 1-vinyl 2-pyrrolidone in the synthesis of AgNPs		58
	2.3.3	Role of Ethylene glycol di-acetate in the synthesis of Ag-NPs		58
	2.3.4	Antimicrobial activity of noble metal nanoparticles and their multi-metallic analogs		60
	2.3.5	3-APTMS mediated synthesis of silver nanoparticles as a function of organic reducing agents		61
	2.3.6	Antimicrobial activity of AgNP-1, AgNP-2, and AgNP-3 against <i>A. baumannii</i>		67
	2.3.7	MIC and MBC determination		68
	2.3.8	Time kill assay		68
	2.3.9	Dose-dependent kill kinetics		69
	2.3.10	Scanning electron microscopic analysis		70
	2.3.11	Fluorescence imaging of silver nanoparticles with <i>A. baumannii</i> cell surface interaction		71
2.4	Discussion			74



2.5	Conclusion	76
Chapter 3:		78-99
Microwave-assisted rapid synthesis and molecular weight of Polyethyleneimine-dependent selective surface interaction and antimicrobial activity of functional silver nanoparticles		
3.1	Introduction	78
3.2	Experimental section	80
	3.2.1	Materials and reagent
	3.2.2	Bacterial strain
	3.2.3	Synthesis of PEI-functionalized silver nanoparticles
	3.2.4	PEI-1 (MW 750,000 Da) and cyclohexanone-mediated synthesis of AgNP-1
	3.2.5	PEI-2 (MW 1300 Da) and formaldehyde-mediated synthesis of AgNP-2
	3.2.6	PEI-3 (MW 60,000 Da) and cyclohexanone-mediated synthesis of AgNP-3
	3.2.7	Synthesis of PEI-mediated Ag-Au bimetallic Nanoparticles
	3.2.8	Characterization of functionalized AgNPs
	3.2.9	Assessment of antibacterial activity and MIC and MBC determinations of Ag-NPs
	3.2.10	Fluorescence spectroscopic studies
	3.2.11	Determination of dynamic quenching of fluorophore fluorescein by PEI-capped AgNPs
	3.2.12	Cell surface-expressed protein–AgNP interaction and membrane fracture studies



3.3	Results		84
	3.3.1	Microwave-assisted Polyethyleneimine-mediated synthesis of silver nanoparticles	84
	3.3.2	Bactericidal activity, minimum inhibitory concentration, and minimum bactericidal concentration of AgNPs	85
	3.3.3	Dynamic fluorescence quenching of fluorescein by PEI-capped AgNPs	88
	3.3.4	Cell surface interaction and membrane breakage of <i>A. baumannii</i> cells by Ag-NPs	89
3.4	Discussion		95
3.5	Conclusions		98
Chapter 4: A whole-cell fluorescence quenching-based approach for the investigation of Polyethyleneimine functionalized silver nanoparticles interaction with <i>Candida albicans</i>			100-122
4.1.	Introduction		100
4.2	Experimental section		102
	4.2.1	Fungal strain, culture media, and growth conditions	102
	4.2.2	Synthesis and physical characterization of PEI-functionalized silver nanoparticles	103
	4.2.3	Assessment of antifungal activity and MIC determination of PEI-functionalized silver nanoparticles	103
	4.2.4	Fluorescence spectroscopic studies	104
	4.2.5	Intracellular ROS generation assay	105



4.3.	Results and discussion		105
	4.3.1	Physical characterization of synthesized Polyethyleneimine functionalized silver nanoparticles	105
	4.3.2	Antifungal activity and minimum inhibitory concentration of PEI-f-Ag-NPs	107
	4.3.3	Fluorescence spectroscopy investigation of cell-nanoparticle binding	109
	4.3.4	Mechanism of FL quenching	111
	4.3.5	Measurement of binding constant and number of binding sites	117
	4.3.6	Antifungal mechanism of PEI functionalized silver nanoparticles	119
4.4.	Conclusions		122
Chapter 5: Size and zeta potential clicked germination attenuation and anti-sporangiospores activity of PEI-functionalized silver nanoparticles against COVID-19-associated Mucorales (<i>Rhizopus arrhizus</i>)			123-155
5.1	Introduction		123
5.2	Experimental Section		126
	5.2.1	Materials and reagent	126
	5.2.2	Fungal strain	126
	5.2.3	Harvesting of sporangiospores	127
	5.2.4	Synthesis and physical characterization of PEI functionalized silver nanoparticles	127
	5.2.5	Assessment of in vitro antifungal activity of silver nanoparticles	128



	5.2.6	Minimum inhibitory concentration (MIC) determination of PEI-f-Ag-NPs	129
	5.2.7	Studies on germination attenuation of sporangiospores	129
	5.2.8	Cell morphology observation with scanning electron microscopy (SEM)	130
	5.2.9	Confocal laser scanning microscopy (CLSM) studies	130
	5.2.10	Raman spectroscopic studies	131
5.3	Results		132
	5.3.1	Synthesis and characterization of PEI functionalized silver nanoparticles	132
	5.3.2	In vitro anti-sporangiospores activity, particularly the effect of PEI-f-Ag-NPs on sporangiospores size and minimum inhibitory concentration value	133
	5.3.3	Sporangiospores germination attenuation studies	138
	5.3.4	Confocal lesser scanning microscopy (CLSM) studies	139
	5.3.5	Ultrastructural investigation of sporangiospores by SEM	140
	5.3.6	Raman spectroscopic studies of PEI-f-Ag-NPs treated sporangiospores	145
5.4	Discussion		147
	5.4.1	Possible anti-sporangiospores mechanism of PEI-f-Ag-NPs	153
5.5	Conclusion		154
Chapter 6: Synthesis of vancomycin functionalized fluorescent gold nanoparticles and selective sensing of mercury (II)			156-172
6.1	Introduction		156



6.2	Experimental Section	159	
	6.2.1	Materials and Methods	159
	6.2.2	Synthesis of vancomycin-loaded Polyethyleneimine functionalized gold nanoparticles	159
	6.2.3	Physical characterization of synthesized nanoparticles (PEI-f-AuNPs@Van)	159
	6.2.4	Sensing of mercury ion (Hg^{2+})	160
	6.2.5	Detection of mercury ion (Hg^{2+}) in an actual environmental sample	160
6.3	Results & Discussion	161	
	6.3.1	Synthesis and characterization of vancomycin-loaded gold nanoparticles	161
	6.3.2	Fluorescence properties of functionalized gold nanoparticles	162
	6.3.3	XPS analysis of vancomycin functionalized gold nanoparticles	164
	6.3.4	PEI-f-AuNPs@Van mediated fluorescence sensing of Hg^{2+}	165
	6.3.5	A plausible mechanism for binding of Hg^{2+} to the PEI-f-AuNPs@Van and physical changes after the addition of Hg^{2+}	166
	6.3.6	Selectivity of PEI-f-AuNPs@Van for Hg^{2+} ions and stability at various parameters	168
	6.3.7	Real environmental sample analysis	170
	6.3.8	Fluorescence lifetime decay analysis	171
6.4	Conclusion	172	
Chapter 7		173-212	



Making vancomycin a potent broad-spectrum antimicrobial agent using Polyaziridine stabilized gold nanoparticle as a delivery vehicle		
7.1	Introduction	173
7.2	Experimental Section	176
	7.2.1 Materials	176
	7.2.2 Microbial Strains	176
	7.2.3 Synthesis and Characterization of Vancomycin Functionalized Gold Nanoparticles	177
	7.2.4 Antimicrobial susceptibility assessment of PEI-AuNP@Van.	177
	7.2.5 Minimal Inhibitory Concentration (MIC) Determination	177
	7.2.6 Microbial growth reduction analysis	178
	7.2.7 Super-resolution confocal Laser Scanning Microscopy studies	178
	7.2.8 Fluorescence Activated Cell Sorting (FACs)	179
	7.2.9 Endogenous Reactive Oxygen Species (ROS) Generation Study	179
	7.2.10 Phosphatidylserine Externalization studies (Apoptosis assay)	180
	7.2.11 Raman Spectroscopy Studies	180
	7.2.12 TEM characterization of PEI-AuNP@Van treated microbial strains	181
7.3	Results	181
	7.3.1 Synthesis and characterization of PEI-AuNP@Van nanoparticles	181



	7.3.2	<i>In-vitro</i> antimicrobial activity of PEI-AuNP@Van nanoparticles	181
	7.3.3	Laser scanning super-resolution Confocal Microscopy (CLSM) Studies	183
7.4	Antimicrobial mechanism studies		188
	7.4.1	Endogenous ROS Generation Studies	188
	7.4.2	Phosphatidylcholine externalization studies	190
	7.4.3	Raman Spectroscopic analysis	192
	7.4.4	Raman spectroscopic analysis of PEI-AuNP@Van and Amphotericin B treated <i>C. albicans</i> and <i>C. tropicalis</i> .	192
	7.4.5	Raman spectroscopic analysis of PEI-AuNP@Van treated cells of <i>E. coli</i> and <i>P. aeruginosa</i>	194
	7.4.6	TEM analysis	196
7.5	Discussion		197
	7.5.1	Assessment of antimicrobial activity of PEI-AuNP@Van	197
	7.5.2	Antimicrobial Mechanism of PEI-AuNP@Van	200
	7.5.3	Intracellular ROS accumulation studies	200
	7.5.4	Raman Spectroscopic studies	201
7.6	Conclusion		204
Chapter 8			
Summary and Future Projections			213-229
References			230-278
List of Publications			279-281



List of Figures

Chapters/ Figure No.	Figure caption	Page No.
Chapter 1		1-45
General Introduction		
1.1	Infographic of the interconnected threat of antibiotic resistance to a different domain of life. Reproduced with permission from CDC under Common Creative attribution license.	3
1.2	A) Bacteria may become antibiotic resistance genes naturally or from the environment. (B) These drug-resistance molecular mechanisms include: i) active efflux of antibiotics outside of the cellular environment through overexpression of efflux pumps, ii) utilization of alternative metabolic pathways to those choked by the drug, iii) decreased permeability of the bacterial cell wall, which blocks the access of antimicrobial agents to target sites, iv) enzymatic cleavage of the antibiotics, v) enzymatic functional group modification of the antibiotic, vi)	4



	modification of antibiotic binding targets, vii) overproduction of the target enzyme to increase the active site competition, and viii) horizontal transfer of resistance genes via quorum sensing signaling within other biofilm-residing bacteria.	
1.3	Schematic representation of the top-down (images with a green background) and bottom-up (images with pale yellow background) approaches of nanoparticle synthesis, the image was adapted from Habibullah et al., 2021.	6
1.4	A) The nano-bio interface and (B) different mechanisms or modes of action of metal nanoparticles against multidrug-resistant microorganisms.	9
1.5	The interfacial interaction model of the Ag-NPs, Ag-NCs, and the bacterial cell membrane. The head groups of the Lipopolysaccharides and DPPE are represented as green sticks; the tails of the Lipopolysaccharides and DPPE are represented as blue sticks. The carboxyl groups and adamantanes are represented as red and cyan sticks. The core Ag and S atoms are represented as yellow and orange beads. (b) Showing the interaction energy between Ag-	12



	<p>NPs/Ag-NCs and the LPS/DPPE molecules. The negative value represents the attraction, and the positive value indicates the repulsion. Coulomb shows electrostatic interaction however, VDW represents van der Waals interaction. Adopted with permission (Chen et al. 2020); (c) showing steps of the development of selenium-doped biphasic calcium phosphate nanoparticles with the doping of silver nanoparticles (Ag-SeB-NPs). (d) Representing the antibacterial mechanism of Ag-SeB-NPs. Adopted with permission (Nie et al. 2020)</p>	
1.6	<p>In situ synthesis of copper nanoparticles incorporated functional coating on mussel-inspired dendritic polyglycerol (MI-dPG) has shown long stability and broad-spectrum antimicrobial activity. a) Chemical structure of mussel-inspired dendritic polyglycerol (MI-dPG); b) Mechanism of catechol anchoring and cross-linking. c) Preparation of Cu nanoparticle-incorporated MI-dPG surface coatings using three different methods. MOPS: 3-(N-morpholino)-propane sulfonic acid. d) Schematic contact killing of bacteria on a Cu nanoparticle-incorporated MI-dPG surface coating via an</p>	16



	“attract-kill-release” mechanism. Reproduced with permission (Li et al. 2017) American Chemical Society.	
1.7	Representative structure of bacterial biofilm: Bacterial biofilm is formed due to complex coordinated interactions of microorganisms with the surface. The sequence of events of typical biofilm formation is as follows; (i) Initial surface attachment to the surface through movement appendages like fimbriae, through Pilli and it can be extracellular carbohydrate matrix, (ii) Formation of a monolayer, movement along the surface with formation of micro colonies and (iii) Biofilm maturation and formation of a three-dimensional structure. The whole event is coordinated by the Quorum sensing (QS) system. In this system, a signal molecule is secreted by a cell and responds against the type of signal molecule. The chemical nature of secreted molecules depends on the class of bacteria.	26
1.8	Schematic representation of the interaction of gold and silver nanoparticles with extracellular DNA. (A) Cationic gold and silver nanoparticles and their respective metal ions establish electrostatic, hydrophobic, and Van der Waals interactions with poly-anionic extracellular DNA in the	34



biofilm. (B) In particular, the silver and gold ions form high-affinity interactions with G-C base pairs of eDNA molecules through short-range Van der Waals and hydrophobic forces. (C) To prevent the oxidative damage of DNA, bacterial cell modifies it via phosphor thiolation. In such cases, gold nanoparticles interact through Au-S bonding extracellular DNA. (D) Both silver and gold nanoparticles also can interact with bacterial RNA molecules especially tRNA through electrostatic and Van der Waals interactions. Schematic representation of various molecular level interactions between metal nanoparticles and extracellular matrix proteins. (E) The metallic nanoparticles interact with quorum-signaling protein molecules (e.g., Las R) through electrostatic, hydrophobic, and hydrogen bonding. In this case, nanoparticles selectively interact with ligand binding sites, making them incompetent for cell signaling. (F) metal nanoparticles interact with metabolic proteins and enzymes present in the biofilm through electrostatic, hydrophobic, hydrogen-bonding, Van der Waals, and π - π interactions, causing them to be inactive for metabolism. (G) Metallic nanoparticles interact with membrane proteins such as electron transport systems that collapse the membrane



	<p>potential and ultimately cell death results. (H) Gold and silver nanoparticles also establish interaction with amyloid-forming proteins such as Fap C and sequester its monomer through electrostatic, hydrophobic, and hydrogen bonding. (I) Gold nanoparticles and their leached ions show strong Au-S bonding with thiol-rich proteins. (J) Gold and silver nanoparticles interact via electrostatic and hydrophobic interaction with functional oligomers of specific proteins. Reproduced with permission (Joshi et al. 2020) under a common creative attribution license.</p>	
1.9	<p>Representing the molecular Mechanisms of development of nano-resistance. a) indicating the changes in cell membrane structure and function; b) nanoparticle modification; c) biofilm development; d) induction of the anti-oxidative system; e) regulation of metabolic pathways. Adopted with permission from Zhang et.al. 2020 © Elsevier.</p>	38
1.10	<p>Implications of nano-resistance for a) co-evolution of antibiotic resistance; b) enhanced pathogenicity; and c) induction of community persister. Adopted with permission from Zhang et.al. 2020 © Elsevier.</p>	42
Chapter 2		46-77



Microwave-assisted rapid synthesis and effect of Organic Functionality on the antimicrobial activity of metal nanoparticles		
Figure 2.1	(A) Characterization of Au-NP-1 nanoparticles by UV-visible light spectrophotometry (i), transmission electron microscopy imaging (ii), and selected area electron diffraction (SAED) pattern (iii). (B) Characterization of synthesized Au-NP-2 nanoparticles by UV-visible light spectrophotometry (i), TEM imaging (ii), and selected area electron diffraction pattern (SAED) (iii).	59
Figure 2.2	(A) Characterization of Ag-Au-NP-1 nanoparticles by UV-visible light spectrophotometry (i), transmission electron microscopy imaging (ii), and selected area electron diffraction pattern (SAED) (iii). (B) Characterization of synthesized Ag-Au-NP-2 nanoparticles by UV-visible light spectrophotometry (i), TEM imaging (ii), and selected area electron diffraction pattern (SAED) (iii).	59
Figure 2.3	(A) Characterization of Pd-Ag bimetallic nanoparticles by UV-visible light spectrophotometry (i), transmission electron microscopy imaging (ii), and selected area electron diffraction pattern (SAED) (iii). (B) Characterization of synthesized Pd-Ag-Au trimetallic nanoparticles by UV-visible light spectrophotometry (i), TEM imaging (ii), and selected area electron diffraction (SAED) pattern (iii).	60
Figure 2.4	Antibacterial assessment plates of bi and tri-metallic nanoparticles against <i>A. baumannii</i> by the agar well diffusion method (i-iv), and Zone of inhibition (in mm) (v). TC representing test control (without silver cation).	61



Figure 2.5	(A) UV-visible light spectrophotometry of Ag-NP-1 (i), Ag-NP-2 (ii), and Ag-NP-3 (iii). (B) Transmission electron microscopy images, a selected area diffraction pattern (inset), and size distribution plots of Ag-NP-1 (i & iv), AgNP-2 (ii & v), and Ag-NP-3 (iii & vi). (C) Zeta potential analysis of Ag-NP-1 (i), Ag-NP-2 (ii), and Ag-NP-3 (iii)	63
Figure 2.6	Role of variable concentration of 1-vinyl pyrrolidone, 3-APTMS, and silver nitrate on the synthesis of Ag-NPs.	64
Figure 2.7	Antibacterial assessment plates of AgNP-1, AgNP-2, and AgNP-3 nanoparticles against <i>A. baumannii</i> by the agar well diffusion method. TC representing test control (without silver cation).	67
Figure 2.8	Mean zone of inhibition diameter of each type of nanoparticle against <i>A. baumannii</i> planktonic cells. +C represents positive control, -C represents negative control, and TC represents test control (without silver cations).	68
Figure 2.9	(i) MIC ($\mu\text{g/ml}$) and MBC ($\mu\text{g/ml}$) values of AgNP-1, AgNP-2, and AgNP-3 against <i>A. baumannii</i> planktonic cells. TC represents Test control and NC represents negative control. (ii) Time kill curve of <i>A. baumannii</i> with 1x MIC concentration of each nanoparticle at 37°C under aerobic conditions. Control represented untreated cells. (iii) Time kill curve of <i>A. baumannii</i> with 1x MBC concentration of each type of nanoparticle at 37°C under aerobic conditions.	69



	Control is represented as untreated cells. (iv) The dose-dependent kill curve at different concentrations of AgNP-1, AgNP-2, and AgNP-3 against <i>A. baumannii</i> after six hours of treatment at 37°C under aerobic conditions; log reduction cfu/ml represents the log value of cfu/ml killed at their corresponding concentration (iv).	
Figure 2.10	Scanning electron microscopy images of control (a), AgNP-1 treated cells (b), AgNP-2 treated cells (c), and AgNP-3 treated cells (d) for 1 hour at respective MIC value in MHB medium at 37°C.	71
Figure 2.11	(A) Fluorescence spectra of bovine serum albumin in the absence (1) and the presence of AgNP-1 (2). (B) Fluorescence spectra of <i>A. baumannii</i> in the absence (3) and the presence of AgNP-1 (4).	72
Figure 2.12	3D fluorescence images of bovine serum albumin in the absence (A, B) and the presence (A', B') of AgNP-1. A and A' show the contour images; B, and B' show the surface images. 3D fluorescence images of <i>A. baumannii</i> in the absence (C and D) and the presence (C' D') of AgNP-1. C and D show the contour images; C' and D' show the surface images.	73
Chapter 3		
	Microwave-assisted rapid synthesis and molecular weight of Polyethyleneimine-dependent selective surface interaction and antimicrobial activity of functional silver nanoparticles	78-99



Figure 3.1	(A) Representing the characterization of Synthesized Ag-NPs by UV-Vis Spectrophotometry, AgNP-1 (i), AgNP-2 (ii), and AgNP-3 (iii); (B) Showing the characterization result of synthesized as AgNPs by TEM imaging with their SAED pattern (inset) and size distribution plot; AgNP-1 (i, iv), AgNP-2 (ii, v) and AgNP-3(iii, vi); (C) Representing the Zeta potential analysis of AgNPs. AgNP-1 (i), AgNP-2 (ii) and AgNP-3 (iii).	86
Figure 3.2	Showing the antibacterial property assessment plate (A); MIC and MBC ($\mu\text{g/ml}$) values of each AgNP against <i>A. baumannii</i> planktonic cells (B). TC represents Test control while NC is negative control.	88
Figure 3.3	A- 2D fluorescence dynamic quenching analysis of fluorescein by PEI capped AgNPs in the presence (iii & iv) and in the absence of <i>A. baumannii</i> cells (ii); while (i) showing fluorescein blank. B- Graph showing the quenching and de-quenching (%) of fluorescein by AgNPs in the presence (a); and in the absence of Ag-NP (b); on addition of 10^4 cells/ml (c); and further increased 10^8 cells/ml (d). C- 3D fluorescence imaging of dynamic quenching of fluorescein by AgNP in the presence (iii & iv) and in the absence of <i>A. baumannii</i> cells (ii); with fluorescein blank (i).	90
Figure 3.4	2D fluorescence spectra of <i>A. baumannii</i> and BSA, treated with synthesized AgNPs (1-3) for 1 and 3 hours. A (i) showing the spectra of BSA treated with AgNPs for 1 hour; and cells treated similarly (ii); B (i) showing the	92



	BSA, treated with AgNPs for 3 hours; and cells treated similarly (ii).	
Figure 3.5	(A) Showing the 3D fluorescence contour plot of BSA (5 $\mu\text{g/ml}$) (i); treated with AgNP-1-3 (5 $\mu\text{g/ml}$) (ii-iv) for 1 hour at room temperature.	93
Figure 3.6	(B) Showing the 3D fluorescence contour plot of bare <i>A. baumannii</i> cells (10^6 cells/ml) (i); treated with AgNP-1-3 (5 $\mu\text{g/ml}$) (ii-iv) for 1 hour at room temperature.	94
Figure 3.7	Representing the 2D Fluorescence spectra of supernatant of 6 hours treated cells with AgNPs (1-3).	94-95
Chapter 4		
A whole-cell fluorescence quenching-based approach for the investigation of Polyethyleneimine functionalized silver nanoparticles interaction with <i>Candida albicans</i>		100-122
Figure 4.1	Physical characterization of PEI-f-Ag-NPs. (A) UV-VIS spectra: inset dispersed in water, (B) respective TEM image, (C) XRD diffractogram, (D) size distribution histogram, and (E) Zeta potential distribution.	107
Figure 4.2	(A) Image shows the zone of inhibition of <i>C. albicans</i> by PEI-f-Ag-NPs. Compound light microscopy photographs of PEI-f-Ag-NPs treated <i>C. albicans</i> cells for various times: (B) untreated control; (C) treated for 5 min; (D) 15 min; (E) 30 min; (F) 60 min; (G) 120 min; and (H) 240 min.	108



Figure 4.3	Effect of UV exposure at variable time intervals on bare <i>C. albicans</i> cells intrinsic protein fluorescence.	110
Figure 4.4	FL emission spectra of <i>C. albicans</i> cell surface proteins at various incubation times with and without PEI-f-Ag-NPs. (A) 2D fluorescence emission spectrum, (B) FL quenching ratio by PEI-f-Ag-NPs at various incubation times, (C) FL emission spectra of <i>C. albicans</i> cell surface proteins with increasing concentration of PEI-f-Ag-NPs, and (D) FL quenching ratio with an increasing PEI-f-Ag-NPs concentration.	111
Figure 4.5	2D and 3D FL emission spectra of calcofluor white-stained <i>C. albicans</i> cells at various incubation times treated with PEI-f-Ag-NPs and without treatment: (A) 2D FL emission spectrum, (B) 3D FL spectrum without PEI-f-Ag-NPs (cell control), (C) 3D FL spectrum involving incubation with PEI-f-Ag-NPs for 5 min, (D) 3D FL spectrum involving incubation with PEI-f-Ag-NPs for 15 min, (E) 3D FL spectrum involving incubation with PEI-f-Ag-NPs for 30 min, (F) 3D FL spectrum involving incubation with PEI-f-Ag-NPs for 60 min, (G) 3D FL spectrum involving incubation with PEI-f-Ag-NPs for 120 min, and (H) 3D FL spectrum involving incubation with PEI-f-Ag-NPs for 240 min.	115
Figure 4.6	FL emission spectra of BSA protein at various times with and without PEI-f-Ag-NPs: (A) fluorescence emission spectrum at various incubation times, (B) FL quenching ratio at various incubation times, (C) FL emission spectra with increasing concentration of PEI-f-Ag-NPs, and (D) FL quenching ratio with increasing PEI-f-Ag-NPs concentration.	116



Figure 4.7	FL emission spectra of tyrosine and tryptophan amino acid standards at various concentrations with and without PEI-f-Ag-NPs: (A) fluorescence emission spectrum of tyrosine, (B) FL quenching ratio by PEI-f-Ag-NPs of tyrosine at various concentrations, (C) FL emission spectra of tryptophan at various concentrations of PEI-f-Ag-NPs, and (D) FL quenching ratio at various PEI-f-Ag-NPs concentration.	117
Figure 4.8	(A) Binding constant (K_b) and number of binding sites (n) for PEI-f-Ag-NP with <i>C. albicans</i> (B) Schematic depicts adsorbed PEI-f-Ag-NPs on the surface of <i>C. albicans</i> cells.	119
Figure 4.9	Intracellular ROS level in PEI-f-Ag-NPs treated <i>C. albicans</i> cells. (A) All events (B) Selected events (10000) (C) Unstained Control (D) Stained Control (E) PEI-f-Ag-NPs treated.	120
Figure 4.10	Schematic showing the possible antifungal mechanism of Polyethyleneimine-functionalized silver nanoparticles. The silver nanoparticle interacts with <i>C. albicans</i> cells via two different pathways, which can be direct or indirect. In the direct pathway, the cationic Ag-NPs interact electrostatically with surface structural proteins and phosphor-mannolipids; these processes induce electrostatic stress followed by ROS generation and inactivation of cytoplasmic proteins. In addition, nanoparticle-generated stress induces mitochondrial ROS inside the cell, which damages cytoplasmic biomolecules such as proteins and DNA through oxidation. The ROS can also damage the cell membrane through lipid peroxidation, resulting in membrane	121



	perforation and eventual cell death (steps 1, 2, 3, 5, and 6) as indicated in the diagram. The indirect action involves silver nanoparticles passing through the cell wall/membrane via water channels or other channels and becoming internalized inside the cell. These silver nanoparticles disintegrate the cytoplasmic biomolecules (e.g., structural proteins and enzymes) and nuclear DNA, collapsing cell cytoarchitectural and resulting in cell death (step 4) as indicated in the diagram.	
Chapter 5		
Size and zeta potential clicked germination attenuation and anti-sporangiospores activity of PEI-functionalized silver nanoparticles against COVID-19-associated Mucorales (<i>Rhizopus arrhizus</i>)		123-155
Figure 5.1	Physical characterization of PEI-f-Ag-NPs. (A) UV-Vis spectra of PEI-f-AgNP-1 (i) show an absorption maximum at $\lambda = 420$ nm and PEI-f-AgNP-2 (ii) show an absorption maximum at showing at $\lambda = 408$ nm. (B) Shows the TEM image and size histogram of PEI-f-AgNP-1 (i & iii) as well as the TEM image and size histogram of PEI-f-AgNP-2 (ii & iv).	134
Figure 5.2	Zeta potential distribution of PEI-f-AgNP-1 and 2	135
Figure 5.3	Assessment of anti-sporangiospores activity of PEI-f-Ag-NPs. (a) Wet mounted vegetative body of <i>R. arrhizus</i> with sporangiospores; (b) freshly harvested sporangiospores; (c) sporangiospores treated with amphotericin B for 24 hours; (d) control sporangiospores at 24 hours, (e) treated with PEI-f-AgNP-1 for 24 hours; (f) treated with PEI-f-AgNP-2 for	136



	24 hours, (g) control sporangiospores at 48 hours; (h) treated with PEI-f-AgNP-1 for 48 hours; (i) treated with PEI-f-AgNP-2 for 48 hours; (j) control sporangiospores at 72 hours; (k) treated with PEI-f-AgNP-1 for 72 hours; and (l) treated with PEI-f-AgNP-2 for 72 hours.	
Figure 5.4	(a) Size distribution histogram of PEI-f-Ag-NPs treated sporangiospores. (i) freshly harvested sporangiospores; (ii) fully germinated sporangiospores at 24 hours; (iii) PEI-f-AgNP-1 treated sporangiospores at 24 hours; (iv) PEI-f-AgNP-2 treated sporangiospores at 24 hours; (v) PEI-f-AgNP-1 treated sporangiospores at 48 hours; (vi) PEI-f-AgNP-2 treated sporangiospores at 48 hours, (vii) PEI-f-AgNP-1 treated sporangiospores at 72 hours, and (viii) PEI-f-AgNP-2 treated sporangiospores at 72 hours. (b) Average sporangiospores size during germination at various times (24-72 hours) in PEI-f-Ag-NPs treated and control sporangiospores.	137-138
Figure 5.5	The minimum inhibitory concentration of PEI-f-Ag-NPs against sporangiospores of <i>R. arrhizus</i> . (a) and (b) representing the % sporangiospores germination inhibition by PEI-f-Ag-NPs in a dose-dependent manner (PEI-f-AgNP-1 MIC/4=0.41, MIC/2=0.82, MIC=1.65, 2xMIC= 3.30 $\mu\text{g}/\text{mL}$) and PEI-f-AgNP-2 (PEI-f-AgNP-2 MIC/4=1.62, MIC/2=3.25, MIC=6.50, 2xMIC= 13.0 $\mu\text{g}/\text{mL}$) Data are presented as percent error bar.	139
Figure 5.6	(a). Showing the confocal laser scanning microscopy of <i>R. arrhizus</i> sporangiospores treated with PEI-f-Ag-NPs and	141-143



	control stained with PI dye, for 24 hours along with their respective DIC images. (i, ii) control sporangiospores; (iii, iv) treated with amphotericin B; (v, vi) treated with PEI-f-AgNP-1 and (vii, viii) treated with PEI-f-AgNP-2. (b). Showing the confocal laser scanning microscopy of <i>R. arrhizus</i> sporangiospores treated with PEI-f-Ag-NPs and control stained with PI dye, for 48 hours along with their respective DIC images. Control sporangiospores (i, ii); (iii, iv) treated with PEI-f-AgNP-1 and (v, vi) treated with PEI-f-AgNP-2. (c). Showing the confocal laser scanning microscopy of <i>R. arrhizus</i> sporangiospores treated with PEI-f-Ag-NPs and control stained with PI dye, for 72 hours along with their respective DIC images. (i, ii) control sporangiospores; (iii, iv) treated sporangiospores with PEI-f-AgNP-1; and (v, vi) treated with PEI-f-AgNP-2.	
Figure 5.7	Scanning electron microscopy images of sporangiospores: (a) control, (b) treated with PEI-f-AgNP-1, and (c) treated with PEI-f-AgNP-2 for 24 hours.	144
Figure 5.8	Elemental analysis (EDS) of sporangiospores: (a) control, (b) treated with PEI-f-AgNP-1, and (c) treated with PEI-f-AgNP-2 for 24 hours.	145
Figure 5.9	Comparison of the surface-enhanced Raman spectra of <i>R. arrhizus</i> sporangiospores treated with PEI-f-Ag-NPs for 24 hours. (i) Raman spectrum of mycelium, (ii) SERS spectrum of freshly harvested sporangiospores, (iii) SERS spectrum of sporangiospores incubated with PEI-f-AgNP-1, and (iv) SERS spectrum of sporangiospores incubated with PEI-	147



	AgNP-2 with corresponding confocal Raman microscopic photographs (inset). Band peaks are assigned for matched biomolecules.	
Figure 5.10	Diagrammatic representation of the possible mechanism of anti-sporangiospores activity of PEI-functionalized silver nanoparticles.	154
Chapter 6		
Synthesis of vancomycin functionalized fluorescent gold nanoparticles and selective sensing of mercury (II)		156-172
Figure 6.1	(A) Real-time UV-visible spectra of vancomycin-loaded Polyethyleneimine functionalized Au-NPs synthesis, (B) corresponding X-ray diffractogram, (C) TEM micrograph, and (D) size distribution plot.	162
Figure 6.2	(A) Hydrodynamic radii of vancomycin-loaded and unloaded gold nanoparticles, (B) zeta potential, (C) fluorescent spectra of vancomycin and vancomycin-loaded gold nanoparticles excited at 270 nm, and (D) fluorescence screening of vancomycin-loaded gold nanoparticles at various excitation wavelengths (270-340 nm).	163
Figure 6.3	XPS spectra of the fluorescent Au-NPs: (A) survey scan showing the presence of various elements, (B) O1s spectra, (C) Au 4f spectra, (D) C1s spectra, and (E) N1s spectra.	164
Figure 6.4	(A) Dependence of Fluorescence emission intensity on Hg^{2+} concentration between 2 and 64 μM , and (B) Stern-Volmer (S-V) plot with the addition of Hg^{2+} under similar conditions	166



	into vancomycin loaded Au-NPs. The inset of Figure 4B shows the kinetic parameters.	
Figure 6.5	(A) Dependence of Fluorescence emission intensity on Hg^{2+} concentration between 2 and 64 μM , and (B) Stern-Volmer (S-V) plot with the addition of Hg^{2+} under similar conditions into vancomycin loaded Au-NPs. The inset of Figure 4B shows the kinetic parameters.	167
Figure 6.6	Stability of PEI-f-AuNPs@Van in different salts (A); on variable pH (B); and effect of time on the fluorescence (C).	168
Figure 6.7	Selectivity of PEI-f-AuNPs@Van against the tested heavy metal analytes.	169
Figure 6.8	(A) Relationship between the fluorescence emission intensity and spiked Hg^{2+} concentration between 0.5-32 μM , and (B) Stern-Volmer (S-V) plot with addition of Hg^{2+} under similar conditions into vancomycin-loaded Au-NPs. The inset of Figure 8B shows the kinetic parameters.	170
Figure 6.9	The time-resolved fluorescence lifetime of PEI-f-AuNPs@Van incubated with and without Hg^{2+} .	171
Chapter 7		
	Making vancomycin a potent broad-spectrum antimicrobial agent using PEI-stabilized gold nanoparticles as a delivery vehicle	173-212
Figure 7.1	Representing the Agar well diffusion plates antimicrobial assessment of PEI-AuNP@Van and mean zone of Inhibition	182



	graph plot; (a) <i>C. albicans</i> , (b) <i>C. tropicalis</i> , (c) <i>E. coli</i> , (d) <i>P. aeruginosa</i> and (e) Mean zone inhibition graph.	
Figure 7.2	Representing the MIC values of vancomycin functionalized gold nanoparticles (PEI-AuNP@Van), against <i>C. albicans</i> , <i>C. tropicalis</i> , <i>E. coli</i> & <i>P. aeruginosa</i> .	183
Figure 7.3	Representing localization of PEI-AuNP@Van around treated cells by using confocal microscopy along with DIC panels. (a) DIC panel of <i>C. albicans</i> (b) blue emission panel of PEI-AuNP@Van treated cells, (c) merged panel; (d) DIC panel of <i>C. tropicalis</i> (e) blue emission panel of PEI-AuNP@Van treated cells, (f) merged panel; (g) DIC panel of <i>E. coli</i> (h) blue emission panel of PEI-AuNP@Van treated cells, (i) merged panel; (j) DIC panel of <i>P. aeruginosa</i> , (k) blue emission panel of PEI-AuNP@Van treated cells and (l) merged panel.	184
Figure 7.4	Representing the intracellular localization of PEI-AuNP@Van nanoparticles inside the cell of <i>C. albicans</i> (a) and <i>C. tropicalis</i> (b), along with Red/blue panels and DIC panels.	185
Figure 7.5	Representing the confocal microscopy along with DIC images of PEI-AuNP@Van treated cells of <i>C. albicans</i> (a & b); <i>C. tropicalis</i> (c & d); <i>E. coli</i> (e & f) and <i>P. aeruginosa</i> (g & h).	186
Figure 7.6	Representing histogram of cell Viability assay, using PI as a probe against PEI-AuNP@Van treated microbial strains. (a) Showing untreated and treated histograms of <i>C. albicans</i> ; (b) Showing untreated and treated histograms of <i>C. tropicalis</i> ;	187



	(c) Showing untreated and treated histograms of <i>E. coli</i> and (d) Showing untreated and treated histograms of <i>P.aeruginosa</i> .	
Figure 7.7	Representing histogram of endogenous ROS generation assay of PEI-AuNP@Van treated strains. (a) untreated control of <i>C. albicans</i> , (b) treated cells; (c) untreated control of <i>C. tropicalis</i> , (d) treated cells; (e) untreated control of <i>E. coli</i> , (f) treated cells; (g) untreated control of <i>P.aeruginosa</i> and (h) treated cells.	189
Figure 7.8	Representing Phosphatidylcholine externalization assay by using Annexin-V/PI system. (a) DIC panel of <i>C. albicans</i> , (b) green panel, (c) red panel; (d) DIC panel of <i>C. tropicalis</i> , (e) green panel, (f) red panel; (g) DIC panel of <i>E. coli</i> , (h) green panel, (i) red panel; (j) DIC panel of <i>P. aeruginosa</i> , (k) green panel and (l) red panel.	191
Figure 7.9	Raman spectrometry of PEI-AuNP@Van exposed microbial cells along with positive control (Amphotericin B and Meropenem) and untreated cells. (a) <i>C. albicans</i> (i) Raman spectrum of untreated cell control; (ii) treated with amphotericin B and (iii) treated with PEI-AuNP@Van. (b) <i>C. tropicalis</i> , (i) Untreated cell control; (ii) treated with Amphotericin B and (iii) treated with PEI-AuNP@Van. (c) <i>E. coli</i> , (i) Untreated cell control; (ii) treated with Meropenem, and (iii) treated with PEI-AuNP@Van. (d) <i>P. aeruginosa</i> , (i) Untreated cell control; (ii) treated with Meropenem, and (iii) treated with PEI-AuNP@Van.	195



Figure 7.10	Representing TEM imaging of PEI-AuNP@Van treated cells of <i>C. albicans</i> , <i>C. tropicalis</i> , <i>E. coli</i> , and <i>P. aeruginosa</i> . (a) Untreated control of <i>C. albicans</i> , (e) PEI-AuNP@Van treated; (b) untreated control of <i>C. tropicalis</i> , (f) PEI-AuNP@Van treated; (c) untreated control of <i>E. coli</i> , (g) PEI-AuNP@Van treated; (d) untreated control of <i>P. aeruginosa</i> and (h) PEI-AuNP@Van treated.	196
Figure 7.11	Possible mode of action of PEI-AuNP@Van against gram-negative <i>E. coli</i> and <i>P. aeruginosa</i> .	204



List of Schemes

Scheme No.	Title	Page No.
Scheme 2.1	Chemical structure of 3-APTMS and 3-GPTMS	47
Scheme 2.2	Chemical structure of cyclohexanone, 1-vinyl 2-pyrrolidone, and ethylene glycol diacetate respectively.	52
Scheme 2.3	Schematic representation of the chapter's work.	76
Scheme 3.1	Chemical structure of branched polyethyleneimine.	79
Scheme 3.2	Representing the possible mechanism of dynamic quenching behavior of PEI-capped AgNPs to fluorescein and interaction affinity towards <i>A. baumannii</i> cells.	91
Scheme 3.3	Representing predicted model of bactericidal mechanism of PEI capped AgNPs.	98
Scheme 5.1	Pathogenesis of <i>R. arrhizus</i> .	125
Scheme 6.1	Chemical structure of Vancomycin	158
Scheme 6.2	Graphical summary of the chapter.	172



List of Tables

Table No.	Title	Page No.
Table 1.1	Metal nanoparticles and associated antimicrobial mechanisms	19
Table 2.1	Physical characteristics of as-prepared mono-, bi-, and trimetallic nanoparticles using 3-APTMS as stabilizing agent and cyclohexanone, 3-GPTMS & formaldehyde as reducing agent.	62
Table 2.2	Effect of variable concentration of 3-APTMS/3-GPTMS on the LSPR of silver and gold nanoparticles prepared in methanol under microwave irradiation.	65
Table 3.1	The physicochemical property of as prepared PEI stabilized silver nanoparticles and respective MIC & MBCs against <i>A. baumannii</i> .	85
Table 3.2	The influence of PEI concentration on the LSPR and absorbance intensity of as-prepared AgNPs.	96
Table 7.1	Raman band assignments of PEI-AuNP@Van treated microbial strains (- indicating the absence of Raman peak and + representing the presence of Raman peak)	205

